

## Supporting Information

### **Biomass-Derived High-Performance Tungsten-Based Electrocatalyst on Graphene for Hydrogen Evaluation**

Fanke Meng,<sup>a</sup> Enyuan Hu,<sup>a</sup> Lihua Zhang,<sup>b</sup> Kotaro Sasaki,<sup>a,\*</sup>

James T. Muckerman,<sup>a</sup> and Etsuko Fujita<sup>a,\*</sup>

<sup>a</sup> Chemistry Department, Brookhaven National Laboratory, Upton, New York, 11973, USA.

<sup>b</sup> Center for Functional Nanomaterials, Brookhaven National Laboratory, Upton, New York 11973, USA

## Experimental

### 1 Synthesis of tungsten-based composite catalysts

Graphene-supported tungsten-based composites ( $\text{WSoy}_x\text{GnP}_y$ ,  $x$  and  $y$  are mass ratios of the soybean and graphene nanoplatelets) were prepared by sintering powdered mixtures of graphene nanoplatelets (GnP,  $x\text{GnP}^{\text{®}}$  C-750 from XG Sciences) with ammonium tungstate (AMT,  $(\text{NH}_4)_{10}\text{H}_2(\text{W}_2\text{O}_7)_6 \cdot 4\text{H}_2\text{O}$ , Aldrich) and soybean (organic yellow dry soybeans supplied by the Whole Food Market, Inc.) powder.

The mass ratio of soybean over AMT was optimized firstly. The detailed procedure is described as follows. First, the soybean was ground to a powder and mixed with AMT. The mass ratios of soybean over AMT were 0.2, 0.5, 0.7, 1.0, and 2.0 respectively. For a typical example, 200 mg of AMT was mixed with 40 mg, 100 mg, 140 mg, 200 mg, and 400 mg of soybean respectively. Second, the mixtures were added into deionized (DI) water and ultrasonicated for 40 min to form uniform suspensions. Third, the suspensions were dried in an oven at 90 °C overnight. Fourth, the dried powders were sintered at 850 °C in argon for 2 hrs in a quartz tube furnace to obtain black catalyst powders for the following experiments. Among all the samples ( $\text{WSoy}_{0.2}$ ,  $\text{WSoy}_{0.5}$ ,  $\text{WSoy}_{0.7}$ ,  $\text{WSoy}_{1.0}$  and  $\text{WSoy}_{2.0}$ ), the  $\text{WSoy}_{0.7}$  exhibited the smallest overpotential ( $\eta_{10}$ ). Consequently, the content of graphene was tuned in the order of  $\text{WSoy}_{0.7}\text{GnP}_{0.5}$ ,  $\text{WSoy}_{0.7}\text{GnP}_{1.0}$  and  $\text{WSoy}_{0.7}\text{GnP}_{2.0}$ . As a comparison,  $\text{WGnP}_{1.0}$  was synthesized using the same method.

### 2 Electrochemical measurements

The electrochemical polarization curves of the catalyst samples were measured with VersaSTAT 3 Potentiostat (Princeton Applied Research) in a three-electrode configuration cell, in which the catalyst, platinum and  $\text{Ag}/\text{AgCl}/\text{KCl}$  (3 M) acted as working electrode, counter electrode and reference electrode, respectively. All potentials were quoted with respect to reversible hydrogen electrode (RHE), and all the polarization curves were  $iR$ -corrected according to ohmic resistance obtained in the electrochemical impedance spectroscopy (EIS) measurement. Typically, 10 mg of catalyst powder was mixed with 5 drops of 20 % Nafion dispersion (DuPont) to form homogenous slurry. The slurry was pasted onto 1  $\text{cm}^2$  carbon paper (Toray TGP-H-060. The size of the carbon paper was 1 cm  $\times$  3 cm, on which a 1  $\times$  1  $\text{cm}^2$  area was exposed for slurry loading). After dried, the carbon paper loaded with catalyst was immersed into

0.1 M HClO<sub>4</sub> (aq.) electrolytes for electrochemical experiments. As a reference, the Pt/C was loaded onto a carbon paper electrode (diameter of 3 mm). The Pt/C (plot (g) in Figure 1(a)) was commercially available from BASF Inc. (20 % HP Pt on Vulcan XC-72R). The electrolyte solution was always bubbled with H<sub>2</sub> during the measurements.

The polarization curves for the hydrogen evolution reaction (HER) were obtained at a scan rate of 2 mV s<sup>-1</sup>. The long-term stability tests were performed by potential cycling between -0.5 V and +0.3 V at a scan rate of 200 mV s<sup>-1</sup>. The EIS measurements were conducted with a frequency from 100000 Hz to 0.01 Hz to determine ohm resistance ( $R_s$ ) and charge-transfer resistance ( $R_{ct}$ ). The double layer capacitances were tested using a glassy carbon electrode with a sample loading of 10 mg cm<sup>-2</sup>.

### 3 Material Characterization

The morphology of the samples was obtained by transmission electron microscope (TEM, JEOL JEM 2100F). To prepare the TEM sample, 2 mg of catalyst was dissolved into 5 mL ethanol by ultrasonication for half minute to achieve a uniform suspension. Then, the suspension was dropped onto a carbon grid (Ted Pella, Inc.), which was thereafter dried in air for observation under TEM. The crystal structure and phase composition were obtained by a high-resolution TEM (HRTEM) and X-ray diffraction (XRD, Rigaku Ultima III) with Cu K $\alpha$  radiation ( $\lambda = 1.542 \text{ \AA}$ ). The three phases in the catalysts were assigned to be  $\alpha$ -W<sub>2</sub>C,  $\delta$ -WC, and WN with the major XRD peaks at 39.6° (101) (JCPDS: 35-0776), 35.6° (100) (JCPDS: 72-0097), 37.7° (111) (JCPDS: 65-2898), respectively. Thermogravimetric Analysis (TGA, Perkin Elmer Diamond) was conducted by heating the samples in oxygen flow (100 sccm) up to 950 °C from room temperature. Then, the samples were kept in oxygen at 950 °C for 10 min to ensure that all the samples were changed to tungsten oxide. The contents of each phase in the catalysts were calculated by using Rietveld-refined XRD spectra and TGA results.<sup>1</sup> The method of Rietveld refinement is briefly introduced in the following experimental section 4.

### 4 Rietveld refinement of the XRD data

Rietveld refinement was carried out using the software GSAS-EXPGUI.<sup>2,3</sup> The refinement is based on the model that physically describes the peak position and peak intensity and semi-empirically describes the peak shape. The peak position is mainly determined by the

lattice constant and x-ray wavelength according to Bragg's law and the peak intensity is mainly determined by atomic positions, atomic vibrations and phase fraction. The peak shape is modeled using a pseudo-Voigt function which is a linear combination of Gaussian function and Lorentzian function. Physical parameters and parameters of describing the peak shape are refined to yield the most satisfactory description of the whole XRD pattern. Phase fraction information is thus obtained.

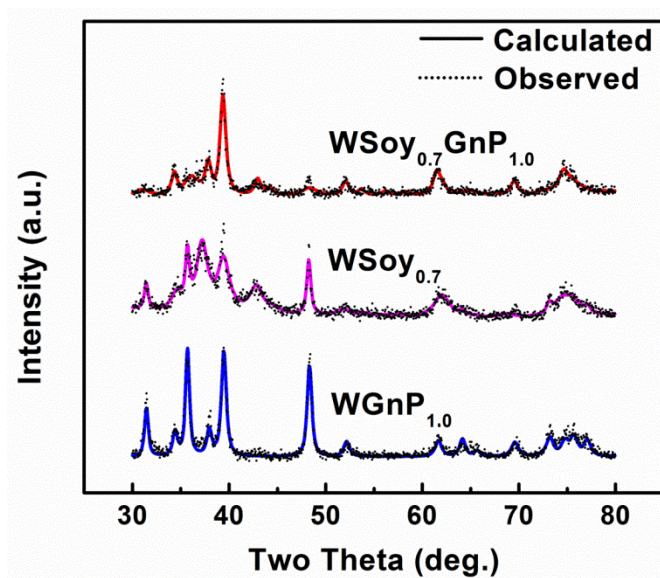


Figure S1. XRD spectra of the samples and Rietveld refined spectra

Table S1. Mass ratio of the  $W_2C$ , WC and WN phases in  $WSoy_{0.7}GnP_{1.0}$ ,  $WSoy_{0.7}$  and  $WGnP_{1.0}$ .

Sample	$WSoy_{0.7}GnP_{1.0}$	$WSoy_{0.7}$	$WGnP_{1.0}$
$W_2C$	0.74	0.44	0.46
WC	0.18	0.46	0.54
WN	0.08	0.1	--

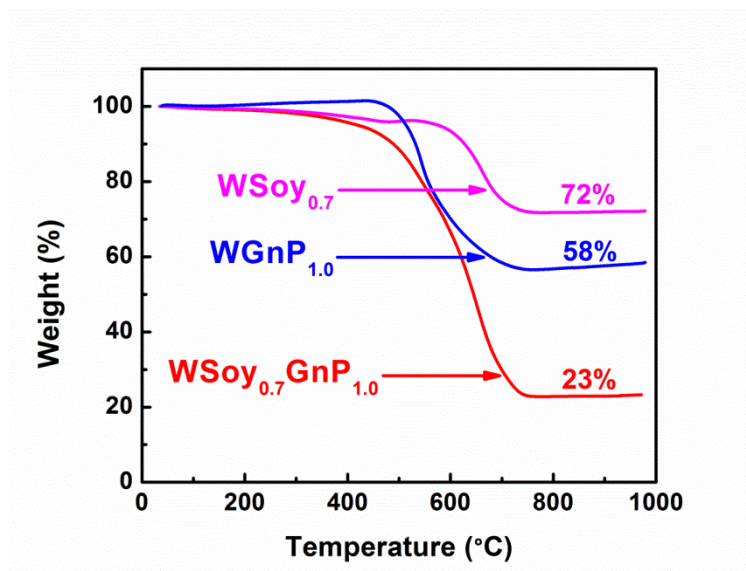
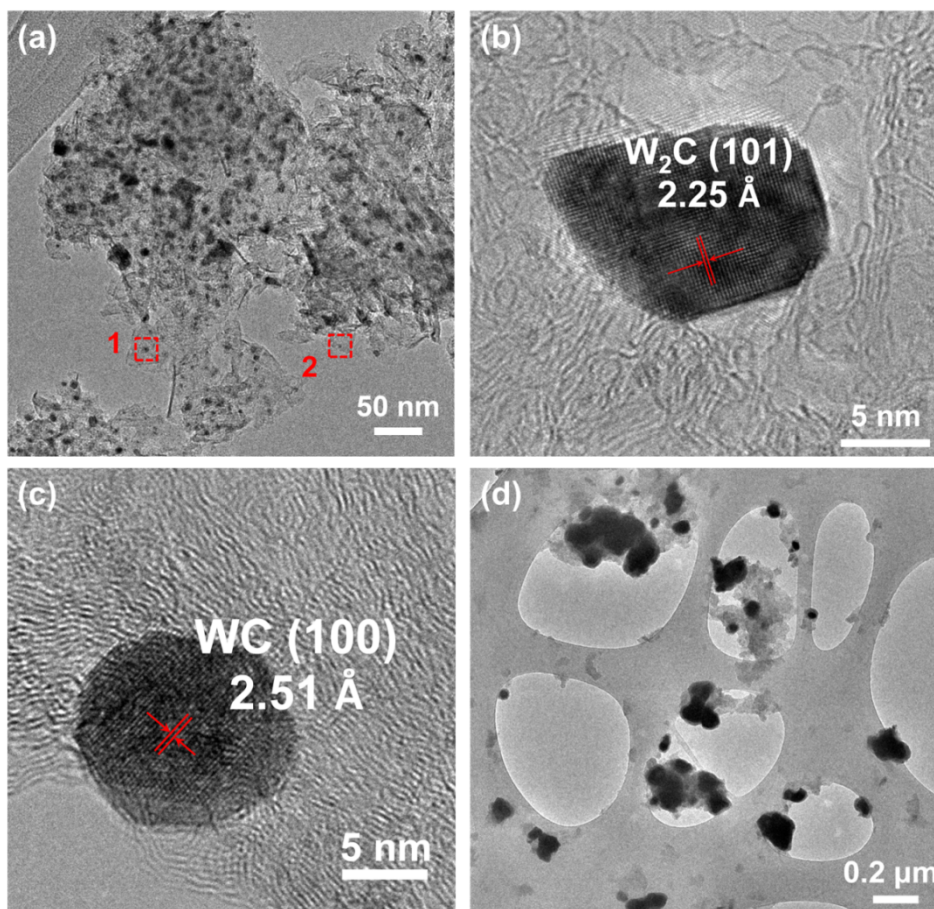
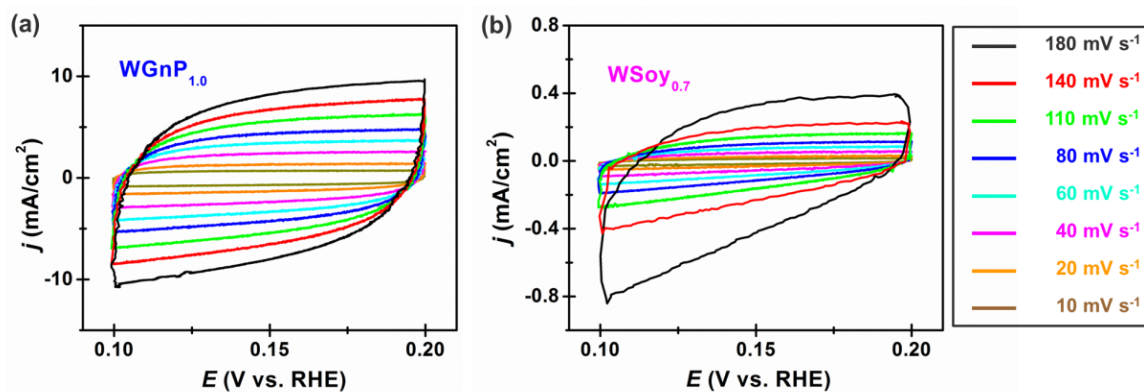


Figure S2. TGA thermograms of the WSoy<sub>0.7</sub>GnP<sub>1.0</sub>, WSoy<sub>0.7</sub> and WGnP<sub>1.0</sub> samples.



**Figure S3.** TEM and HRTEM images of the WGNP<sub>1.0</sub> (a)-(c), and WSoy<sub>0.7</sub> (d). The HRTEM images in (b) and (c) show the area of the red squares labeled 1 and 2, respectively, in image (a) indicating decoration of W<sub>2</sub>C and WC nanoparticles on the graphene nanoplatelets.



**Figure S4.** Cyclic voltammetry curves of the WGNP<sub>1.0</sub> and WSoy<sub>0.7</sub> in the region of 0.1-0.2 V.

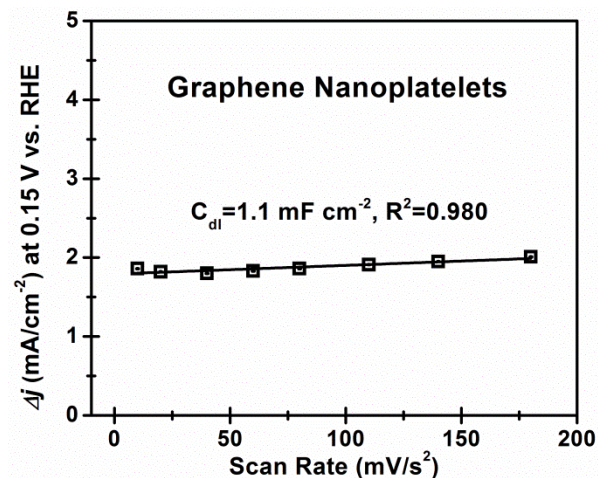


**Figure S5.** Linear fitting of the capacitive current of the graphene nanoplatelets vs. the scan rate to obtain the  $C_{dl}$ .

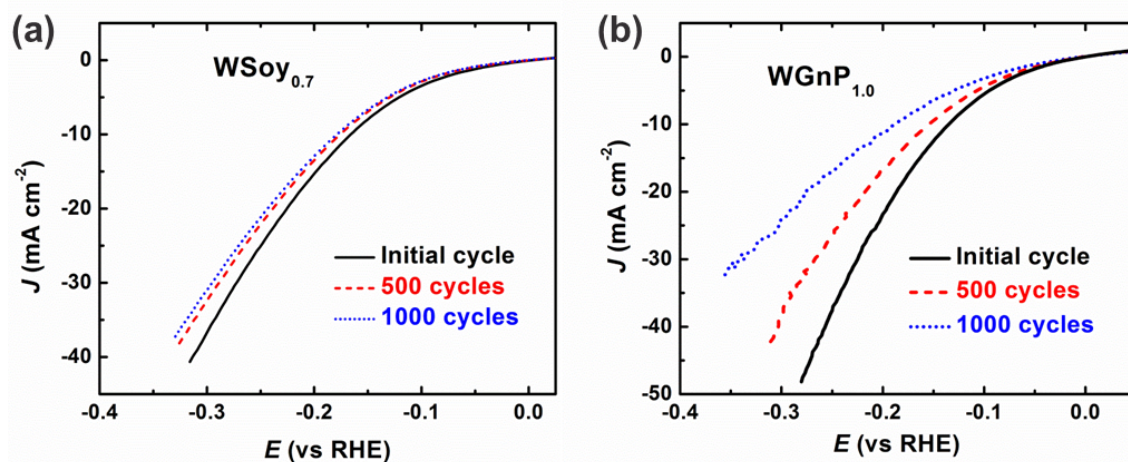


**Figure S6.** Polarization curves of the  $WSoy_{0.7}$  and  $WGnP_{1.0}$  catalysts before and after 500 and 1000 cycles at potentials between -0.5 V and +0.3 V with a scan rate of  $200 \text{ mV s}^{-1}$ .

Table S2. Comparison of different W-based HER electrocatalysts available from literatures.

Catalyst	Overpotential ( $\eta_{10}$ ), mV	Tafel slope, mV dec <sup>-1</sup>	Exchange Current Density, 10 <sup>-2</sup> mA cm <sup>-2</sup>	R <sub>ct</sub> , $\Omega$	Stability	Ref.
WSoy <sub>0.7</sub> GnP <sub>1.0</sub>	105	36	6.3	10.7 @ 100 mV	1000 cycles, 24 hrs Chronopotentialmetric electrolysis, stable	This study
$\alpha$ -WC/carbon black	260	N/A	N/A	N/A	3000 cycles, stable	4
W <sub>2</sub> C microsphere	~ 170 (a)	118	28.1	N/A	N/A	5
Commercial WC	~ 300 (a)	73	1.8	N/A	N/A	5
W <sub>0.5</sub> Ani/GnP	120	68.6 (b)	3.8	12.7@100 mV	10000 cycles, stable	1
W <sub>2</sub> C/GnP	186	64.7 (b)	2.4	15.6@100 mV	5000 cycles, not stable	1
Bulk W <sub>2</sub> C	336	88.0 (b)	0.065	1750@100 mV	N/A	1
WN	>500	N/A	N/A	N/A	5000 cycles, stable	1
Thin film W <sub>2</sub> C	>300 (c)	69	0.02	N/A	N/A	6
Thin film WC	> 400 (c)	91	0.25	N/A	N/A	6
WS <sub>2</sub> nanosheets	~ 160	72	0.25	N/A	1000 cycles, stable	7
Exfoliated 1T WS <sub>2</sub>	~260 (a)	~55	2.0	>250 @100 mV	>10000 cycles, stable	8
WS <sub>2</sub> /rGO hybrid nanosheets	~260 (a)	58	<0.1 (d)	~200	N/A	9
metallic WS <sub>2</sub> nanosheets	142	70	N/A	5 @250 mV	500 cycles, slight loss in catalytic activity	10
WS <sub>2</sub> nanoflakes	~150 (a)	48	N/A	N/A	10000 cycle, slight loss in catalytic activity	11
WS <sub>2</sub> nanoribbons	225	68	1.25	38 @250 mV, >2000 @100 mV	1000 cycle, stable	12
WSe <sub>2</sub> on carbon fiber paper	300	77.4	N/A	N/A	15000 cycle, stable	13
WSe <sub>2</sub>	~350 (a)	99	0.3	624 @128 mV	Potentiostatic electrolysis for 7000 s, stable	14

W(S <sub>0.48</sub> Se <sub>0.52</sub> ) <sub>2</sub>	~260 (a)	105	2.9	204@128 mV	Potentiostatic electrolysis for 7000 s, stable	14
Amorphous WP	~120 (a)	54	4.5	N/A	500 cycles 18 hr, 100 mV/s stable	15
P-modified WN/rGO	85	54	35	N/A	5000 cycles, slight loss in catalytic activity	16
WC on vertically aligned CNTs	145	72	~10 (d)	N/A	1000 cycles, slight loss in catalytic activity	17

(a) The overpotential ( $\eta_{10}$ ) was estimated from *JV* polarization curves.

(b) The Tafel slope was obtained from plots of *E* vs.  $\log(R_{ct})^{-1}$ .

(c) The overpotential ( $\eta_{10}$ ) was estimated from Tafel plots.

(d) The exchange current density was estimated from Tafel plots.

## References

- (1) W. F. Chen, M. S. Schneider, K. Sasaki, C. H. Wang, J. Schneider, S. Iyer, S. Iyer, Y. Zhu, J. T. Mucherman and E. Fujita, *ChemSusChem*, 2014, **7**, 2414–2418.
- (2) "Gsas." General Structure Analysis System, A.C. Larson, R.B. Von Dreele. LANSCE, MS-H805, Los Alamos, New Mexico (1994).
- (3) EXPGUI, a graphical user interface for GSAS, B.H. Toby, *J. Appl. Crystallogr.*, 2001, **34**, 210-213.
- (4) S. T. Hunt, T. Nimmanwudipong and Y. Roman-Leshkov, *Angew. Chem. Int. Ed.*, 2014, **53**, 5131–5136.
- (5) D. J. Ham, R. Ganesan and J. S. Lee, *Int. J. Hydrogen Energy*, 2008, **33**, 6865–6872.
- (6) D. V. Esposito, S. T. Hunt, Y. C. Kimmel and J. G. Chen, *J. Am. Chem. Soc.*, 2012, **134**, 3025–3033.
- (7) Z. Wu, B. Fang, A. Bonakdarpour, A. Sun, D. P. Wilkinson and D. Wang, *Appl. Catal., B.*, 2012, **125**, 59–66.
- (8) D. Voiry, H. Yamaguchi, J. Li, R. Silva, D. Alves, T. Fujita, M. Chen, T. Asefa, V. B. Shenoy, G. Eda and M. Chhowalla, *Nat. Mater.*, 2013, **12**, 850–855.

- (9) J. Yang, D. Voiry, S. J. Ahn, D. Kang, A. Kim, M. Chhowalla and H. Shin, *Angew. Chem. Int. Ed.*, 2013, **52**, 13751–13754.
- (10) A. S. Daniel, C. R. English, F. Meng, A. Forticaux, R. J. Hamers and S. Jin, *Energy Environ. Sci.*, 2014, **7**, 2608–2613.
- (11) L. Cheng, W. J. Huang, Q. F. Gong, C. H. Liu, Z. Liu, Y. G. Li and H. J. Dai, *Angew. Chem. Int. Ed.*, 2014, **53**, 7860–7863.
- (12) J. Lin, Z. Peng, G. Wang, D. Zakhidov, E. Larios, M. Yacaman and J. M. Tour, *Adv. Energy Mater.*, 2014, **4**, 1301875.
- (13) H. T. Wang, D. S. Kong, P. Johannes, J. J. Cha, G. Y. Zheng, K. Yan, N. Liu and Y. Cui, *Nano Lett.*, 2013, **13**, 3426–3433.
- (14) K. Xu, F. M. Wang, Z. X. Wang, X. Y. Zhan, Q. S. Wang, Z. Z. Cheng, M. Safdar and J. He, *ACS Nano*, 2014, **8**, 8468–8476.
- (15) J. M. McEnaney, C. Crompton, J. F. Callejas, E. J. Popczun, C. G. Read, N. S. Lewis and R. E. Schaak, *Chem. Commun.*, 2014, **50**, 11026–11028.
- (16) H. Yan, C. Tian, L. Wang, A. Wu, M. Meng, L. Zhao, H. Fu, *Angew. Chem. Int. Ed.*, 2015, **54**, 6325–6329.
- (17) X. Fan, H. Zhou, X. Guo, *ACS Nano*, 2015, **9**, 5125–5134.